# A complete and easily accessible means of calculating surface exposure ages or erosion rates from $^{10}$Be and $^{26}$Al measurements

Greg Balco [a,d,*] John O. Stone [a] Nathaniel A. Lifton [b]
Tibor J. Dunai [c]

[a] *Quaternary Research Center and Department of Earth and Space Sciences University of Washington, Mail Stop 351310, Seattle, WA 98195-1310 USA*

[b] *Geosciences Department, University of Arizona, Tucson, AZ 85721 USA*

[c] *University of Edinburgh, School of GeoSciences, Institue of Geography Drummond Steet, Edinburgh, EH8 9XP United Kingdom*

[d] *Present address: Berkeley Geochronology Center 2455 Ridge Road, Berkeley, CA 94709 USA*

**Abstract**

We codify previously published means of calculating exposure ages and erosion rates from $^{10}$Be and $^{26}$Al concentrations in rock surfaces, and present a single complete and straightforward method that reflects currently accepted practices and is consistent with existing production rate calibration measurements. It is intended to enable geoscientists, who wish to use cosmogenic-nuclide exposure age or erosion rate measurements in their work, to: a) calculate exposure ages and erosion rates; b) compare previously published exposure ages or erosion rate measurements on a common basis; and c) evaluate the sensitivity of their results to differences between published production rate scaling schemes. The method is available online at *http://hess.ess.washington.edu*.

*Key words:* Cosmogenic nuclide geochronology, beryllium-10, aluminum-26, exposure dating, erosion rate measurements,

* Corresponding author. Tel. 206-221-2579
*Email address:* balcs@u.washington.edu (Greg Balco).

## 1 Introduction

In this paper we describe a complete method for calculating surface exposure ages and erosion rates from measurements of the cosmic-ray-produced radionuclides $^{10}$Be and $^{26}$Al in surface rock samples. It is available online via any web browser at the following URL:

*http://hess.ess.washington.edu/*

This method codifies previously published procedures for carrying out the various parts of the calculation. The importance of this contribution is not that we present significant improvements over previous calculation schemes, but that we have combined them with all published production rate calibration measurements in an internally consistent fashion, and made the resulting method easily accessible via an online system. This system is intended to enable geoscientists who seek to use cosmogenic-nuclide exposure ages or erosion-rate measurements in their work to: a) calculate exposure ages and erosion rates; b) compare previously published exposure ages or erosion rate measurements on a common basis; and c) evaluate the sensitivity of their results to differences between published production rate scaling schemes. This contribution is part of the CRONUS-Earth project, an initiative funded by the U.S. National Science Foundation whose goal is to improve Earth science applications of cosmogenic-nuclide geochemistry. It also reflects collaboration with the CRONUS-EU project, an initiative with similar goals funded by the European Union.

This project is motivated in the first place by the fact that the number of applications of cosmogenic-nuclide measurements, as well as the number of papers published on the subject, is growing rapidly. These studies are no longer being carried out exclusively by specialists in cosmogenic-nuclide geochemistry, but by Earth scientists who wish to apply cosmogenic-nuclide methods in a wide variety of studies. These methods are still in active development, so a variety of data-reduction procedures, reference nuclide production rates, and production rate scaling schemes exist in the literature. Many of these schemes are at least in part inconsistent with each other, and yield different results for the same measurements of nuclide concentrations. The effect of this has been that published exposure-age and erosion-rate data sets lack a common basis for comparison. For example, even without regard to the absolute accuracy of any of the exposure-age calculation methods relative to the true calendar year time scale, the variety of inconsistent methods makes it difficult to directly compare the results of any two exposure-dating studies. This, in turn, is a serious obstacle for paleoclimate research or any other broader research task which relies on synthesizing the results of many studies. We seek to address this situation by providing an easily accessible means of comparing new and previously published exposure ages or erosion rates in a consistent fashion.

The primary goal of this system is to provide an internally consistent result that reflects commonly accepted practices. At present, it is impossible to evaluate whether or not it will always yield the 'right answer,' that is, for example, the correct calendar age for exposure-dating samples of all locations and ages. There are still many uncertainties in the present understanding of nuclide production rates and scaling factors, and there are certain to be future improvements in understanding of the physics behind production rate calculations as well as in the quality and coverage of production rate calibration measurements. This means that the exposure age that we infer from a particular measurement of nuclide concentration, at a particular location, will change as production rate calculation methods improve. In nearly all cases, the exposure age calculated with this system from a published $^{10}$Be or $^{26}$Al measurement will differ from the age reported in the original paper. Future versions of this system that reflect improved understanding of nuclide production rates will, in turn, yield different results from the present version. Our goal is to ensure that, at any time, it will be possible to recalculate old and new measurements with a common method.

The second goal of this project is to standardize the entire array of published production rate scaling schemes to a common set of calibration measurements. Papers reporting cosmogenic-nuclide measurements commonly parameterize nuclide production rates by a reference production rate at sea level and high latitude. This hides the important fact that a stated reference production does not in fact reflect a single direct measurement at sea level and high latitude, but a normalization of many geographically scattered measurements. Thus, a reference production rate implies both a set of calibration measurements and a scaling scheme used to normalize them. When one seeks to measure the erosion rate or exposure age at a new site, the scaling scheme used to scale the reference production rate to the new site must be the same as the scaling scheme that was used to normalize the calibration measurements. If these two parts of the calculation are not consistent, the exposure age or erosion rate will be incorrect. Furthermore, in order to compare exposure ages for the same site that result from two different scaling schemes, one must make sure that the two scaling schemes have been normalized to the same calibration data set. Both of these standardizations require a systematic compilation of calibration data, which has not been widely available to date. Here we have compiled such a data set, and used it to ensure not only that the results of using a single scaling scheme are internally consistent, but also that the results from the entire suite of scaling methods are based on a single calibration data set.

Finally, the system we describe here is intended to serve as a foundation for future improvements. Overall, the objective of the CRONUS-Earth and CRONUS-EU projects is to improve the accuracy of exposure age and erosion rate measurements in two ways: first, by better understanding the physical processes involved in cosmogenic-nuclide production; second, by improving the production rate calibration data set to better constrain production rates and scaling methods. The online exposure-age and erosion-rate calculators are intended to provide an outlet for the

results of this work.

## 2 Description of the exposure-age calculator

### *2.1 System architecture*

The exposure age and erosion rate calculator is based on MATLAB software. MATLAB itself provides a high-level programming language designed for mathematical computation. It is useful for this purpose because: i) it minimizes the need for low-level coding of numerical methods; ii) it is commonly used by geoscientists; and iii) MATLAB code is easier to understand than lower-level programming languages.

We have chosen to use a central server, rather than distributing a standalone application that runs on a user's personal computer (e.g., CALIB: Reimer et al., 2004), because: i) the web-based input and output scheme is platform-independent; ii) the existence of only a single copy of the code minimizes maintenance effort and ensures that out-of-date versions of the software will not remain in circulation; and iii) the fact that all users are using the same copy of the code at a particular time makes it easy to trace exactly what method was used to calculate a particular set of results.

The software consists of two main components: a set of web pages that act as the user interface to the software, and a set of MATLAB functions ('m-files') that check input data, carry out calculations, and return results. In this paper, we describe the general features of the calculation method, that is, the key equations, parameter values, and reference data, and discuss important assumptions and limitations of the methods. A detailed description of all the MATLAB code, including full mathematical descriptions of the calculations as well as a discussion of the accuracy of the numerical methods, is accessible through the web site and is included as supplementary material with this article.

The underlying MATLAB code is freely accessible through the web site (subject to the terms of the GNU General Public License, version 2, as published by the Free Software Foundation). We intend that the existing functions can serve as building blocks for users who wish to carry out more elaborate calculations than are possible using the relatively restricted set of input forms.

### *2.2 Inputs*

*Direct observations vs. calculated values.* Table 1 shows the measurements and observations needed to calculate an exposure age or an erosion rate from $^{10}$Be or

$^{26}$Al concentrations. In general, the calculator is designed to take only direct observations and measurements as input to the exposure age and erosion rate calculations. Our goal has been to make sure that all derived or calculated quantities are produced internally within the calculation, so that exposure ages or erosion rates computed with this system cannot be rendered inconsistent by differences in how the input data were generated. However, there are two exceptions to this rule: the 'shielding factor' and the $^{26}$Al and $^{10}$Be concentrations. Here we discuss these two input parameters, as well as the different options for entering site elevations and/or atmospheric pressures, in more detail.

*Shielding factor.* The calculation of corrections for topographic or geometric obstructions that reduce the cosmic ray flux to the sample site takes place outside the main exposure age or erosion rate calculation. That is, the calculators take as input a derived 'shielding factor' rather than direct observations of the horizon geometry, which presents the possibility that shielding factors computed using different methods could introduce an inconsistency in the results. We have done this for two reasons. First, there is no standard format for recording exposure geometry, and the complexity of the horizon description required for an accurate computation differs greatly between different samples. Second, we are aware of only very few publications that include detailed horizon descriptions (most report only calculated shielding factors), so if this information were required as input it would be difficult to recalculate exposure ages or erosion rates from most published measurements.

Corrections for horizon obstructions are generally computed using the approach introduced by Nishiizumi et al. (1989) and nearly universally adopted thereafter, which assumes that the angular distribution of the cosmic radiation responsible for $^{26}$Al and $^{10}$Be production decreases in proportion to $\cos^{(2.3)}(\theta)$, where $\theta$ is the zenith angle. Gosse and Phillips (2001) discuss the choice of the exponent in more detail. One then determines the fraction of the total cosmic-ray flux that is obstructed by integrating this function over the portion of the upper hemisphere that is below the horizon imposed on the sample site by the surrounding topography. The 'horizon' seen by the sample is usually taken to be that imposed by obstructions that are more than several effective attenuation lengths for spallogenic production – that is, at least several meters – thick. In practice this means that this method of calculating the shielding factor is used to account for both topographic features at the scale of tens of meters or greater, and for situations in which the sample is located in the center of a gently dipping surface that is at least meters to tens of meters wide. We provide a separate online calculator, external to the main exposure age or erosion rate calculation, for calculating shielding corrections according to this set of assumptions.

This approach conceals a number of major simplifications, which are insignificant for most sample sites, but become important in three situations: i) when the sample site is surrounded by small obstructions with spacing and thickness comparable to the attenuation length for spallogenic production; ii) when sample sites are heavily

shielded, that is, a significant fraction of the upper hemisphere is obstructed; and iii) when sample sites are steeply dipping ($>\sim 30^\circ$) or strongly convex. In these situations, our present approach could cause future systematic errors if an improved method of calulating geometric shielding were introduced, but existing publications did not contain enough information to fully recalculate shielding factors using the improved method. We suggest that authors working in unusual geometric situations report not only calculated shielding factors, but detailed descriptions of the geometry of their sample sites as well.

*Nuclide concentrations.* The calculator takes as input a nuclide concentration (atoms $\cdot$ g$^{-1}$), rather than a raw isotope ratio measurement. Users must convert the Be or Al isotope ratios measured by AMS into nuclide concentrations before input. In other words, we separate the calculation of the nuclide concentration itself from the computation of an exposure age or erosion rate from that nuclide concentration. Calculating the nuclide concentrations requires not only the raw Be or Al isotope ratio of the sample, but also information about the quantity and isotope ratio of the carrier solutions used, a variety of Al and Be concentration measurements made on samples and carrier solutions, the concentrations of stable and radio-isotopes in reagent and process blanks, and the isotope ratios of primary and secondary standards used in the AMS measurements. Deriving the nuclide concentrations in the sample quartz from this information depends too heavily on internal laboratory standards and procedures for us to provide a standard interface. We have provided an outline of how to calculate nuclide concentrations from isotope ratio measurements in the online documentation. Also, we anticipate that future efforts to standardize the reporting format for AMS results may make it possible to move part or all of this calculation online.

*AMS measurement standards.* An additional aspect of nuclide concentration measurements that is important to the exposure age and erosion calculations is the fact that Be and Al isotope ratio measurements are made by comparison to a reference standard with a defined isotope ratio. In order to maintain consistency between calculated exposure ages or erosion rates and the calibration data set, nuclide concentrations submitted to the calculator must be normalized to a reference standard that is compatible with the reference standard used in the calibration measurements. The measurements in our calibration data set are referenced to standards that are compatible with the Be and Al isotope ratio standards described in Nishiizumi (2002) and Nishiizumi (2004) (henceforth, the 2002 Nishiizumi Be standard and the 2004 Nishiizumi Al standard). If measurements of nuclide concentration submitted to the online calculators are not also compatible with these standards, the resulting exposure ages or erosion rates will be incorrect. These standards, or compatible ones, are widely used at many AMS facilities. However, results from some AMS laboratories may need to be renormalized before they are submitted to the online calculators.

Published intercomparison studies suggest some situations where renormalization

may be needed, and we summarize these briefly here. However, this is not an exhaustive list, and users who need further information should consult the AMS laboratory where their measurements were made. With regard to $^{26}$Al measurements, Nishiizumi (2004) and Wallner et al. (2000) compared Al isotope ratio standards in use at various AMS laboratories. These studies suggest that $^{26}$Al measurements made against some standards in use at ETH-Zurich and University Köln may need to be adjusted for use with the online calculators. With regard to $^{10}$Be measurements, several AMS laboratories use, or have used in the past, a National Institute of Standards and Technology (NIST) Be isotope ratio standard whose certified value is not consistent with the 2002 Nishiizumi Be standard. Thus, $^{10}$Be measurements referenced to the NIST standard may need to be renormalized before they are submitted to the calculators. Nishiizumi et al. (2007) discuss this issue in detail. In addition, there are likely to be significant changes in $^{10}$Be reference standards in common use in the near future. Nishiizumi et al. (2007) remeasured the isotope ratio of the material used for the 2002 Nishiizumi Be standards and found that it differed from the value stated in Nishiizumi (2002). This is likely to lead to a change in the reporting of $^{10}$Be measurements at many AMS laboratories.

*Elevation and atmospheric pressure.* The calculators provide several different means of specifying the sample elevation. The sample elevation is important because it determines the atmospheric depth at the site, which is the environmental factor that has the largest effect on nuclide production rates. As the atmospheric depth, not the elevation, is the factor controlling production rates, the measurement that is actually needed to compute the production rates is the mean atmospheric pressure at the site during the period of exposure. Unfortunately, this is difficult to determine accurately because i) sample sites are rarely located adjacent to long-term weather observing stations, and ii) most sample sites are much older than instrumental records of atmospheric pressure, so the modern observations are unlikely to reflect the true mean pressure throughout their full exposure duration. The site elevation, on the other hand, is easy to measure accurately. Thus, most studies report the elevations of sample sites, and use a standard pressure-elevation relationship, typically the ICAO standard atmosphere, to determine the site pressure. The standard atmosphere is designed to approximate the typical atmospheric density structure at mid-latitudes; however, many features of global air circulation cause persistent geographic variations, as well as temporal changes associated with long-term climate and sea-level change, in the pressure-height relationship. This means that applying the standard atmosphere universally will result in important errors in exposure ages and erosion rates in many parts of the world. Stone (2000), Dunai (2000), Farber et al. (2005), and Staiger et al. (2007) discuss this in more detail.

This calculator allows users to enter either atmospheric pressure or elevation for their sample sites. If elevation is entered, it provides a choice of atmosphere approximations to convert elevation to atmospheric pressure. For sites in Antarctica, users should choose a height-pressure relationship from Radok et al. (1996); Stone (2000) discusses the relationship between this and the standard atmosphere in de-

tail. For sites outside Antarctica, we provide a default atmosphere approximation that uses the basic formula of the standard atmosphere, but incorporates geographically variable mean sea level pressure and 1000 mbar temperature fields as a means of capturing regional variations in the height-pressure relationship. The mean sea level pressure and 1000 mbar temperature fields are from the NCEP-NCAR reanalysis (*www.cdc.noaa.gov/ncep_reanalysis/*). Henceforth we refer to this scheme as 'our default height-pressure relationship.' We evaluated this scheme by comparison to actual mean annual pressures observed at 2873 meteorological stations in the National Center for Atmospheric Research, World Monthly Surface Station Climatology data set (NCAR Data Set ds570.0; *http://dss.ucar.edu/datasets/ds570.0/*). The $^{10}$Be production rate calculated using our default height-pressure relationship is within 5% of the $^{10}$Be production rate calculated from the observed pressure at 96% of the stations (Figures 1, 2). In addition, our default height-pressure relationship corrects a systematic underprediction of the production rate at high elevations that results from applying the ICAO standard atmosphere globally (Figure 1), and slightly improves the fit of some scaling schemes to the production rate calibration data set relative to the ICAO standard atmosphere. Stations where our default height-pressure relationship does a poor job of predicting the measured atmospheric pressure are mainly located in high-relief continental areas, for example in the Andes and Central Asia (Figure 2). There are many such areas, however, so users who require accurate exposure-dating results are best served by making a serious effort to determine the mean atmospheric pressure at their sites from nearby station data, rather than from global approximations (e.g., Farber et al., 2005). It is also important to note that we have made no effort to account for temporal variations in atmospheric pressure. Staiger et al. (2007) discusses this issue in detail.

*Importance of reporting direct measurements and observations as well as derived ages and erosion rates.* Finally, the fact that methods of calculating exposure ages and erosion rates are certain to change in future highlights the critical importance of reporting raw observations as well as derived ages or erosion rates. We cannot emphasize enough that the results derived from a particular set of measurements will be superseded by future improvements, and if a study does not report enough information to update the results using improved methods, it will be effectively useless to future researchers. Table 1 provides a checklist of the observations and measurements that are needed to calculate an exposure age or erosion rate, and the input web pages provide links to sample spreadsheets that contain all the necessary information. In practice, we suggest that publications that report exposure ages and erosion rates provide equivalent spreadsheets as a table or appendix.

### *2.3 Outputs*

The exposure age and erosion rate calculations return two sets of results:

(1) *Version information.* The result page identifies the version of each component of the software that was active at the time. Users should keep track of these version numbers as a record of exactly what calculation method was used.
(2) *Results of the calculation.* Tables 2 and 3 describe these. We discuss the difference between internal and external uncertainties in detail in Section 2.8.

### *2.4 Physical constants and input parameters used throughout the calculations*

The physical constants and parameters that are used in the calculation fall into three categories: reference nuclide production rates derived from calibration measurements, which are described in the next section; constants specific to particular parts of the calculation, which are described in the documentation for individual MATLAB functions; and parameters that are widely used throughout the calculations, which we describe here.

*Effective attenuation length for spallation in rock.* We take the effective attenuation length for production by high-energy spallation in rock (henceforth $\Lambda_{sp}$) to be 160 $g \cdot cm^{-2}$ always. Gosse and Phillips (2001) review measurements of $\Lambda_{sp}$ in detail.

*Decay constants.* The absolute isotope ratios assigned to the 2002 Nishiizumi Be standard and the 2004 Nishiizumi Al standard, to which we have normalized our calibration measurements, also imply particular values for the $^{26}$Al and $^{10}$Be decay constants. Thus, our choice of values for the decay constants is determined by our choice of measurement standards. These values are $4.62 \times 10^{-7}$ $yr^{-1}$ and $9.83 \times 10^{-7}$ $yr^{-1}$ for $^{10}$Be and $^{26}$Al respectively (Nishiizumi, 2002, 2004). Note that the redetermination by Nishiizumi et al. (2007) of the isotope ratio of the 2002 Nishiizumi Be standard also implies a larger value for the $^{10}$Be decay constant. Thus, the value of the $^{10}$Be decay constant adopted here may be incorrect. However, it is still required in the context of the online calculator to ensure consistency between $^{10}$Be production rates and $^{10}$Be measurements that are both referenced to the 2002 Nishiizumi standards. As noted by Nishiizumi et al. (2007), adopting the revised values for the isotope ratio of the Be reference standard and the $^{10}$Be decay constant would result in a negligible change to relatively young exposure ages (order $10^4$ yr), because restandardization of nuclide concentrations at calibration sites and unknown sites will offset each other, but would result in a significant change to older (order $10^6$ yr) exposure ages. To summarize, this issue is of limited importance for many exposure-dating applications, but is potentially significant for long exposure times and slow erosion rates. Future modifications to the online calculators will most likely be required to take account of this and other measurements of the $^{10}$Be decay constant.

### *2.5 Production-rate scaling schemes*

Calculating cosmogenic-nuclide production rates at a sample site requires two things: first, a scaling scheme that describes the variation of the production rate with time, location, and elevation; and second, a reference production rate at a particular time and place, usually taken to be the present time, sea level, and high latitude. This reference production rate is not measured directly, but is determined by: i) measuring nuclide concentrations in surfaces of known exposure age, which yields a set of local, time-averaged production rates; ii) using the scaling scheme to scale these local, time-averaged production rates to the present time at sea level and high latitude; and iii) averaging the resulting set of reference production rates to yield a best estimate of the true value. Given a particular set of calibration measurements, each scaling scheme yields one and only one best estimate of the reference production rate, and each scaling scheme will yield a different such estimate. In other words, we know the local, time-integrated, production rates at the calibration sites accurately, and then seek to tie them together using a set of scaling equations that has one free parameter, the reference production rate. For each scaling method, there is a different value of that parameter that best reproduces the measured local production rates. The important point is that a reference sea-level high-latitude production rate is not an absolute or independent constant, but implies a particular set of calibration measurements and a particular scaling scheme.

In this section, we describe the scaling schemes for different nuclide production pathways that we use in the calculators. In the following section, we describe the set of calibration measurements used to obtain the reference production rates for each scaling scheme. We make no attempt here to describe the individual scaling schemes in more than general terms; readers are referred to the supplementary material, the online documentation, and the source papers for complete details.

Production of $^{26}$Al and $^{10}$Be takes place by three mechanisms: high-energy spallation, negative muon capture, and fast muon interactions, each of which vary differently with time and location. We use only a single scaling scheme for nuclide production by muons. We calculate production rates due to fast muon interactions according to Heisinger et al. (2002b), and production rates due to negative muon capture according to Heisinger et al. (2002a). As suggested in these papers, we scale muon production rates for elevation using energy-dependent atmospheric attenuation lengths from Boezio et al. (2000). We do not consider magnetic field effects on the muon flux; thus, production due to muons does not vary with latitude or with time. This simplification does not introduce significant inaccuracies because the production rate due to muons varies only by ca. 15% over the relevant range of cutoff rigidity values. This is much smaller than the variation in production due to muons with altitude (an approximate doubling every 2000 m). As production by muons is never more than a few percent of total surface production of $^{26}$Al or $^{10}$Be, this simplification does not have a significant effect on the exposure age or erosion

rate calculations.

On the other hand, we use five different scaling schemes for nuclide production by high-energy spallation. These are listed in Table 4. This results in a suite of five different exposure age or erosion rate results for each sample. Presenting multiple scaling schemes is intended to accomplish two things: first, to give an idea of how strongly a conclusion drawn from exposure-age or erosion-rate results depends on the assumptions of the particular scaling scheme that was used; second, to help in future development of scaling methods by identifying locations and ages where different scaling schemes diverge significantly, and therefore where development efforts ought to be targeted.

The simplest scaling scheme that we use, that of Stone (2000) following Lal (1991) (henceforth, the 'St' scheme) describes variation in spallogenic production rates with latitude and atmospheric pressure, and assumes that the production rate is constant through time. This scaling scheme was developed by Lal (1991), who described the variation of nuclide production rates with altitude and latitude. Stone (2000) then recast these scaling factors as functions of atmospheric pressure rather than altitude without changing the basic scaling relationships (note that Stone (2000) also corrected a typographical error in Table 1 of Lal (1991)). This was the earliest production-rate scaling scheme available, and is by far the most commonly used in the existing literature. It fits the existing calibration data set as well or better than any other (see discussion below). However, the surface cosmic ray flux depends on the strength of the Earth's magnetic field, and the strength of the Earth's magnetic field is known to have varied in the past. Hence, production rates must have varied over time, and the St scaling scheme cannot account for this variation. This deficiency, as well as the fact that measurements of the modern near-surface cosmic ray flux are now more extensive than the early data sets used by Lal, led several researchers to develop alternative scaling methods: these are the scaling schemes of Dunai (2001) (henceforth, 'Du'), Desilets et al. (2006) ('De') and Lifton et al. (2005) ('Li'). These differ from the St scheme in two important ways: first, they predict a significantly different elevation dependence for spallogenic production; second, they account for changes in production rates due to magnetic field changes (De, Du, and Li) and solar variability (Li). Finally, in an effort to separate the difference in altitude scaling from the difference between the time-dependent and non-time-dependent scaling schemes, we have also implemented a fifth scaling scheme that retains the altitude scaling of Lal (1991), but adds a simple paleomagnetic correction based on Nishiizumi et al. (1989) (the 'Lm' scaling scheme).

We determine the reference production rates for all the scaling schemes using a single calibration data set (discussed below), and we use a single set of magnetic field reconstructions as input to the time-dependent scaling schemes. The magnetic field reconstruction is similar to that used by Lifton et al. (2005), with the addition of spherical harmonic field models for the last 7000 years from Korte and Constable (2005a). The scaling schemes that take account of magnetic field effects define

production rate variations not as a function of primary magnetic field properties, but as a function of geomagnetic cutoff rigidity (the minimum energy that an incoming primary particle must have to generate a particle cascade in the atmosphere at a particular location), and the different scaling schemes calculate the cutoff rigidity from the magnetic field reconstruction in different ways. Note that the Lm scaling scheme cannot accommodate longitudinal variation in cutoff rigidity, because the Lal (1991) scaling factors on which it is based are defined as a function of latitude rather than cutoff rigidity. Thus, the spherical harmonic magnetic field model we use for the Holocene must be reduced to an geocentric dipole field in applying this scaling scheme. Table 5 summarizes the magnetic field reconstructions as well as the methods of calculating past values of cutoff rigidity.

The difference between exposure ages and erosion rates calculated using the different scaling schemes varies with location, elevation, and the duration of surface exposure. In general terms, the major differences are as follows:

(1) The magnetic field reconstructions that we use in the calculators portray the recent magnetic field strength as unusually high. This predicts that, at low latitudes where paleomagnetic field changes are important, surfaces that have been exposed for a longer time will have been subject to a higher average production rate. As most of the calibration sites have exposure ages of 10-20 ka, a non-time-dependent scaling scheme will predict a lower production rate than a paleomagnetically-corrected scheme for samples older than the calibration sites, and a higher production rate for samples younger than the calibration sites. This means that for low-latitude sites, the St scaling scheme will yield older exposure ages than the other scaling schemes for samples older than the calibration sites, and younger ages than the other scaling schemes for samples younger than the calibration sites. Figure 3 shows this effect.
(2) Nuclide production rates depend more strongly on elevation in the De, Du, and Li scaling schemes than in the St and Lm scaling schemes. In effect the scaling schemes are fixed to each other by the calibration measurements at moderate elevations, so the De, Du, and Li schemes predict higher production rates at high elevations, and lower production rates at low elevations, than the St and Lm schemes. Thus, De, Du, and Li will yield older exposure ages than St and Lm at low elevations, and younger ages at high elevations. Figure 4 shows this effect.

Other differences between the results produced by the different scaling schemes are smaller, more complex in space and time, and largely stem from: a) the different methods of calculating cutoff rigidities from the magnetic field reconstructions, and b) small diffferences in the placement of the latitudinal "knees," that is, the critical values of cutoff rigidity at which the cosmic-ray flux begins to change rapidly.

Note that several of the source papers (Dunai, 2000; Lifton et al., 2005) for the individual scaling schemes include plots and contour maps that compare different

scaling methods. These comparisons all fix the scaling schemes being compared so that they yield the same production rate at the reference location of sea level and high latitude. Here we have fixed all of the scaling schemes not to a single value at sea level and high latitude, but to a common set of geographically widespread calibration measurements. Thus, using the online calculators to compare different scaling schemes will not duplicate previously published comparisons. The geographic and temporal variation in predicted production rates will be similar, but the absolute differences in production rates or exposure ages will not.

### *2.6 Production rate calibration*

*The calibration data set.* $^{26}$Al and $^{10}$Be production rates due to muons are fully specified from muon flux observations and interaction cross-sections by Heisinger et al. (2002b) and Heisinger et al. (2002a). Production rates due to spallation, on the other hand, must be calibrated by measuring nuclide concentrations in sites of known age. We used a set of calibration measurements that is similar to that used by Stone (2000). This includes only published measurements, from Nishiizumi et al. (1989), Gosse and Klein (1996), Gosse et al. (1995), Stone et al. (1998a), Larsen (1996), Nishiizumi et al. (1996), Kubik et al. (1998), Kubik and Ivy-Ochs (2004) and Farber et al. (2005). John Gosse provided additional data on sample locations and geometries that are not reported in Gosse et al. (1995) or Gosse and Klein (1996). Of these studies, Nishiizumi et al. (1989), Gosse et al. (1995), Larsen (1996), and Kubik et al. (1998) included $^{26}$Al as well as $^{10}$Be measurements, but we did not use the $^{26}$Al measurements from Kubik et al. (1998) due to the possibility of a standardization inconsistency with the other measurements (Nishiizumi, 2004). We have corrected a standardization error in Stone et al. (1998a) and renormalized their results to the 2002 Nishiizumi Be standards. To the best of our knowledge, all the measurements in the calibration data set are consistent with the 2002 Nishiizumi Be standards and the 2004 Nishiizumi Al standards. In this work, we have done our best to apply recent improvements in the radiocarbon time scale (Reimer et al., 2004) to the limiting radiocarbon ages for some of the calibration sites. The calibration data set appears in the supplementary material.

We used the following chain of reasoning in averaging the calibration measurements to determine the reference production rate and its uncertainty for each scaling scheme. First, we assume that all the individual measurements at a particular calibration site are scattered only because of measurement error. Thus, we scale all the measurements from a single site to the reference location, and take the error-weighted mean of the resulting estimates of the reference production rate to arrive at a summary estimate of the reference production rate measured at that site. However, we do not know if scatter among the reference production rates estimated at different sites is the result of measurement uncertainty, dating errors in determining the actual exposure ages of the calibration sites, or inaccuracies in the scaling

scheme. Lacking additional knowledge, we simply take the average and standard deviation of the set of summary values from all the sites as the reference production rate to be used in the calculators. This results in a relatively large uncertainty in the reference production rate that conflates random measurement errors, errors in dating or geologic interpretation at the calibration sites, errors in estimating mean atmospheric pressure at the calibration sites, and inaccuracies in the scaling methods or the magnetic field reconstructions. The practical importance of this is that the calculators will overestimate the external uncertainty in exposure ages or erosion rates from sites that are close to the calibration measurements in location and age. In reality, the closer an unknown site is to a calibration site, the smaller the production rate uncertainty ought to be, but we have not attempted to capture this effect.

This is a different averaging procedure than is used in Stone (2000). In that work, each sample was equally weighted; here we weight each site equally. This change in the averaging procedure, the adjustments to some calibrated radiocarbon dates, and additional samples from Larsen (1996) and Farber et al. (2005) account for the small difference between the reference production rates for the St scaling scheme used here (e.g., $4.96 \pm 0.43$ atoms $\cdot$ g$^{-1}\cdot$ yr$^{-1}$ for spallogenic $^{10}$Be production) and in Stone (2000) ($4.99 \pm 0.3$ atoms $\cdot$ g$^{-1}\cdot$ yr$^{-1}$).

The $^{26}$Al calibration data set is much smaller than the $^{10}$Be calibration data set, consisting of only three sites from North America between 37°- 43°N latitude. The reference $^{26}$Al production rates inferred from the $^{26}$Al data set agree with the $^{10}$Be production rates inferred from the full $^{10}$Be data set in that the $^{26}$Al/$^{10}$Be production ratio is in all cases indistinguishable from the established value of 6.1 (Table 5). However, presumably because the $^{26}$Al data set is geographically restricted, the uncertainty in the reference $^{26}$Al production rates inferred from the $^{26}$Al calibration data set is much smaller than the uncertainty in the reference $^{10}$Be production rates, and would probably underestimate scaling uncertainties if applied globally. Thus, for the exposure age and erosion rate calculators, we actually use reference production rates and uncertainties for $^{26}$Al that we obtain by multiplying the reference $^{10}$Be production rates inferred from the $^{10}$Be calibration data set by 6.1. This yields reference $^{26}$Al production rates that are indistinguishable from those inferred directly from the $^{26}$Al measurements, but larger uncertainties that reflect the geographically more comprehensive $^{10}$Be data set.

One potential weakness in the calibration data set is that most of the source papers reported only site elevations and simply used the ICAO standard atmosphere to obtain mean atmospheric pressures. We have improved this somewhat by using our default pressure-altitude relationship described above in section 2.2. Farber et al. (2005) are an exception: they calculated the mean air pressure at their sites from nearby meteorological station records. A better effort to determine mean air pressures for all the calibration sites from nearby station data or regional climate models, as well as to account for past changes in air pressure at ice-marginal sites,

might reduce scatter in the data set. Staiger et al. (2007) discuss this issue in more detail.

*Fit of the scaling schemes to the calibration data.* We can to some extent evaluate the quality of a scaling scheme by looking at how well it fits the calibration data set (Table 5, Figures 5 and 6). The two scaling schemes based on the Lal (1991) scaling factors (St and Lm) fit the $^{10}$Be calibration data marginally better than the three scaling schemes that are based on more recent neutron monitor measurements (De, Du, and Li). However, the nominal difference in fit arises mainly because these latter schemes do not do as good a job of matching a single calibration study, that of Farber et al. (2005) in Peru, to the mid- and high-latitude sites. This is potentially important, because this site is at high elevation and low latitude where scaling schemes differ the most, and comparing this site with high-latitude sites is a critical test of the scaling methods. However, this site is also located in an area where the pressure-height relationship is very different from the standard atmosphere, so how one determines the mean atmospheric pressure makes a significant difference in the results of the fitting exercise. Thus, we are hesitant to take the Peru results as favoring the St and Lm scaling schemes without additional measurements from low latitudes. Overall, this highlights the importance of locating additional calibration sites at low latitudes.

In general, none of the scaling schemes yield a statistically acceptable fit to the calibration data set. In part this must reflect inaccuracies in the scaling schemes themselves, but with the present data set it is impossible to separate scaling scheme errors from possible systematic errors in the calibration measurements themselves, which might arise from errors in the independent dating or from systematic offsets between measurements made at different laboratories.

The fact that the Peru calibration data are an outlier with respect to the De, Du, and Li scaling schemes significantly increases the nominal uncertainty in the reference production rates corresponding to these schemes (Table 5). This suggested that we might be overestimating the uncertainty in the reference production rate by relying too heavily on the Peru data. In an effort to bring more data to bear on this question, we looked at the available $^{3}$He calibration data set as well. Although we are not presenting a $^{3}$He exposure age calculator in the present work, these measurements provide additional information about scaling uncertainties from an entirely independent data set. The $^{3}$He calibration data consist of measurements from Kurz et al. (1990), Cerling and Craig (1994), Licciardi et al. (1999), Dunai and Wijbrans (2000), Ackert et al. (2003), and Licciardi et al. (2006). We used only the samples from Kurz et al. (1990) with good surface preservation, and also discarded samples from very young lavas that had large uncertainties. We followed the example of these and other authors in assuming that there is no $^{3}$He production by muons. We did not include the data from Blard et al. (2006), because they argued persuasively that their method of accounting for a grain-size dependence in $^{3}$He concentrations in crushed minerals rendered their results inconsistent with previous measurements

that were made without regard for grain size. The scaling schemes do not fit the $^{3}$He data set as well as the $^{10}$Be data set, and yield slightly larger uncertainties (11-15%)in the reference production rate (Table 5, Figure 7). A detailed discussion of the reasons for this scatter is well beyond the scope of this paper. Regardless, the scatter in reference production rates inferred from the $^{3}$He data set suggests that we have not overestimated the uncertainty in the $^{26}$Al and $^{10}$Be production rates by relying too heavily on the Peru calibration site.

### *2.7 Exposure ages and erosion rates*

The exposure age calculator solves the equation:

$$N = S_{thick} S_G P_{ref,sp,Xx} \int_0^T S_{Xx}(t) \exp(-\lambda t) \exp\left(\frac{-\epsilon t}{\Lambda_{sp}}\right) dt + P_\mu \int_0^T \exp(-\lambda t) \exp\left(\frac{-\epsilon t - z/2}{\Lambda_\mu}\right) dt \quad (1)$$

for the exposure age $T$. Here $N$ is the measured nuclide concentration in the sample (atoms $\cdot$ g$^{-1}$), $S_{thick}$ is the thickness correction (nondimensional), $S_G$ is a geometric shielding correction (nondimensional), $P_{ref,sp,Xx}$ is the reference production rate due to spallation for scaling scheme Xx (atoms $\cdot$ g$^{-1}\cdot$ yr$^{-1}$), $S_{Xx}(t)$ is the scaling factor (nondimensional) for scaling scheme Xx, which may or may not vary over time depending on the scaling scheme, $\lambda$ is the decay constant for the nuclide in question (yr$^{-1}$), $\epsilon$ is an independently determined surface erosion rate (g $\cdot$ cm$^{-2}\cdot$ yr$^{-1}$), $\Lambda_{sp}$ is the effective attenuation length for spallogenic production (g $\cdot$ cm$^{-2}$), $P_\mu$ is the surface production rate in the sample due to muons (atoms $\cdot$ g$^{-1}\cdot$ yr$^{-1}$), $z$ is the sample thickness (g $\cdot$ cm$^{-2}$), and $\Lambda_\mu$ is an effective attenuation length for production by muons (g $\cdot$ cm$^{-2}$).

The important details of this method as follows:

(1) Production by spallation is taken to have an exponential depth dependence with a single attenuation length.
(2) As discussed above in section 2.5, production by muons is taken to be constant in time.
(3) Production by muons is taken to be unaffected by topographic shielding. This is acceptable because where production by muons is important, that is, at depths great enough so that spallogenic production is insignificant, the muon flux is highly collimated and less affected by geometric shielding than the surface muon flux. This assumption would fail for near-vertical faces or otherwise heavily shielded sites.

(4) The depth-dependence of production by muons is simplified to be exponential with a single attenuation length. This is justified because sites that can be accurately exposure-dated are by definition those where erosion is slow. If erosion is slow, production by muons accounts for a small fraction of the measured nuclide concentration and this simplification is irrelevant.
(5) The depth-dependence of production by muons is taken to be linear within the sample, that is, we take the production rate due to muons at the center of the sample to be the production rate in the entire sample. By similar reasoning as (4), this is acceptable for samples thinner than ca. 20-30 cm.

Equation 1 cannot be solved analytically, so must be solved numerically. Furthermore, as $S_{Xx}(t)$ is defined piecewise, the corresponding integral must be computed numerically. The details of the solution method, as well as the step size and accuracy of the integration methods, appear in the documentation for the MATLAB code (available through the web site) and in the supplementary material. We also use Equation 1 for determining the reference production rates from the calibration data set. but solve for $P_{ref,sp,Xx}$ instead. This can be done analytically except that the first integral in Equation 1 must still be calculated numerically. We use the same integration method as in the exposure age calculation.

The erosion rate calculator solves the equation:

$$N = S_{thick} S_G P_{ref,sp,Xx} \int_0^\infty S_{Xx}(t) \exp\left(-\lambda t\right) \exp\left(\frac{-\epsilon t}{\Lambda_{sp}}\right) dt + \int_0^\infty P_\mu(\epsilon t + z/2) \exp\left(-\lambda t\right) dt \tag{2}$$

for the erosion rate $\epsilon$. There are two key differences between this and Equation 1: first, the erosion rate calculation retains the full depth dependence of production by muons rather than treating it as an exponential with a single attenuation length; second, the integration method is modified somewhat to be numerical with respect to changes in the production rate due to spallation with time only, and to use an exact formula with respect to depth and radioactive decay. Once again, Equation 2 cannot be solved analytically and a numerical solution method must be used.

Most erosion rates calculated from $^{10}$Be and $^{26}$Al concentrations in the existing literature were calculated using the equation of Lal (1991):

$$N = \frac{P_0}{\lambda + \frac{\epsilon}{\Lambda_{sp}}} \tag{3}$$

where $P_0$ is the surface production rate. This assumes that the depth dependence of nuclide production is that of spallation only, and disregards the fact that production

by muons decreases less rapidly with depth. As pointed out by Stone et al. (1998b) and Granger et al. (2001), given that the other assumptions of the method are satisfied, erosion rates calculated using Equation 3 underestimate the true erosion rate by at least a few percent in all cases, and by several tens of percent for low-elevation sites. Thus, the erosion rates calculated using the present method (Equation 2) will be systematically higher than many erosion rate measurements in the existing literature. Figure 8 gives an idea of the significance of this offset.

### *2.8 Error propagation*

*Formal uncertainties.* The challenge in providing a realistic uncertainty for calculated exposure ages and erosion rates is that there are few data available to establish the accuracy of many parts of the calculation. In principle, we ought to include three separate uncertainties in calculating the uncertainty on an exposure age or erosion rate: i) uncertainties in nuclide concentration measurements, ii) uncertainties in the scaling schemes, and iii) uncertainties in the input parameters to the scaling schemes, in particular the reference production rate, the atmospheric pressure at the site, and the magnetic field reconstruction. As the analytical standards to which our calibration measurements are normalized are associated with specific values of the $^{10}$Be and $^{26}$Al decay constants, we do not take account of uncertainty in the decay constants. Also, the decay constant uncertainty makes a negligible contribution to the total uncertainty in most exposure-dating and erosion-rate applications.

Of these three important sources of uncertainty, the magnitude of the measurement uncertainty is directly available from the AMS measurement, but in practice it is difficult to separate uncertainty in the scaling scheme itself from uncertainty in the input parameters to the scaling scheme. First, the source papers describing the scaling schemes vary widely in their treatment of scaling factor uncertainty. Lifton et al. (2005) include formal uncertainties for all their parameters, but Lal (1991), Dunai (2001), and Desilets et al. (2006) only provide general uncertainty estimates. Second, the scaling uncertainties described in these source papers reflect the fit of the scaling schemes to measurements of the modern cosmic-ray flux using neutron monitors or film emulsions. Cosmic rays actually responsible for production reactions in rock may have a different energy spectrum from those recorded by neutron monitors, so it is not clear whether scaling factors that accurately reproduce neutron monitor measurements are equally accurate for scaling production rates in rock. The calibration data set provides a test of this to some extent, but at present it is not extensive or consistent enough to quantitatively separate errors in the scaling scheme from errors in the calibration measurements themselves, the independent dating of the calibration sites, or the atmospheric pressure estimates.

We have chosen to deal with this by taking the scaling schemes and the magnetic field reconstructions used as input to the scaling schemes as precise, and arguing

that the uncertainty introduced by this simplification will be manifested in the scatter among reference production rates inferred from different calibration sites. We then use the magnitude of this scatter to assign an uncertainty to the reference production rate that includes the effects of uncertainties in the scaling scheme and the input parameters to the scaling scheme. In other words, we are assuming that the scatter among reference production rates derived from the individual calibration sites is a good representation of the combined uncertainty in the calibration data themselves, the scaling schemes, and the magnetic field reconstructions. This approach is straightforward and relatively conservative, and has the advantage that the calibration measurements from which the uncertainties are derived are similar in nature to the exposure-age and erosion-rate measurements for which the online calculator is intended. Also, disregarding the formal uncertainties provided in the published magnetic field reconstructions that we use is relatively unimportant to the total uncertainty estimate. This is because, as we are interested in the average production rate during a long period of exposure, point-to-point uncertainties in past magnetic field strength are minimized. We note that the uncertainty in the reference production rates derived in this way is in fact similar in magnitude ($\sim$10%) to the scaling uncertainties suggested in the source papers for the scaling schemes. Overall, we believe that the available data do not support a more complicated approach to error propagation at present. The main disadvantage of this approach, as discussed above, is that in principle we ought to be know production rates more accurately at locations that are close to the calibration sites in time and space, but we cannot do this with the present method.

We report two separate uncertainties for each exposure age or erosion rate calculation. First, the 'internal uncertainty' takes only measurement uncertainty in the nuclide concentration into account. This is useful in situations where one wishes to compare exposure ages or erosion rates derived from $^{26}$Al and $^{10}$Be measurements on samples from a single study area. For example, when asking whether exposure ages of adjacent boulders on a single moraine agree or disagree, one should use the internal uncertainty. Second, the 'external uncertainty' adds the uncertainty in the reference nuclide production rate for spallation (derived from the scatter in the scaled calibration measurements as described above), and the uncertainty in the nuclide production rate by muons (derived from the cross-section measurements in Heisinger et al. (2002a,b)). One should use the external uncertainty when comparing exposure ages from widely separated locations, or for comparing exposure ages to ages generated by other dating techniques. Finally, with regard to comparing exposure ages derived from different cosmogenic nuclides, $^{26}$Al and $^{10}$Be exposure ages calculated here are based on the same production model and calibration data set, so $^{26}$Al and $^{10}$Be exposure ages from closely spaced sites may be compared using the internal uncertainty. $^{3}$He, $^{21}$Ne, $^{36}$Cl, or $^{14}$C exposure ages, on the other hand, are based on different production models and calibration data, so the external uncertainty should be used when comparing them to $^{26}$Al or $^{10}$Be ages calculated here.

We actually calculate the uncertainties by assuming that the uncertainties in the input parameters are normal and independent, and that the result is linear with respect to all of the uncertain parameters, and adding in quadrature in the usual fashion (e.g., Bevington and Robinson, 1992). The main disadvantage of this method is that it does not capture the fact that the actual uncertainties in our results are not symmetrical around the central value. The fact that we cannot incorporate non-ideal probability distributions for the input parameters is a secondary disadvantage, although it is mitigated by the fact that there is little evidence to suggest whether or not the uncertainty in these input parameters is in fact asymmetric or otherwise unusual. Keeping this issue in perspective relative to actual geological applications of cosmogenic-nuclide measurements, we are not aware of any studies where the difference between asymmetrical and symmetrical uncertainties would affect the conclusions of the study.

*Formal uncertainties vs. difference in results from different scaling schemes.* Finally, we discuss the relationship between the formal uncertainty we report for an exposure age calculated using one of the five scaling schemes, and the spread among the results from all the scaling schemes. The purpose of reporting results according to five different scaling schemes is so that users can identify situations where exposure ages are or are not sensitive to the major assumptions that vary between scaling methods. If all the scaling schemes yield the same exposure age – which is mainly true for sites of similar location and age to the calibration sites – the user can have more confidence in the accuracy of the result. Note that the fact that we have estimated the uncertainties in all the reference production rates from the same calibration data set requires that the results of the different scaling schemes will nearly always overlap within their external uncertainties.

In practice, there is no compelling reason for a user to prefer the results from any particular scaling scheme, and there is no strong argument to recommend any one of the scaling schemes for reporting published results. Furthermore, there is no reason to believe that the results from the different scaling schemes are randomly distributed, so averaging them will not yield a more accurate age estimate. As we have already discussed, the most important point to remember when reporting results from these calculators is that users should always report all the input data as well as the derived exposure ages or erosion rates. If all the input data appear in a paper, it is easy for authors, reviewers, or readers to recalculate the ages or erosion rates using any present or future scaling scheme, and thus evaluate how sensitive the authors' conclusions are to production rate scaling assumptions.

## 3 Significant compromises and cautions

Several aspects of calculating exposure ages or erosion rates that we have discussed above involve simplifications or parameterizations for parts of the calculation that:

i) are not well understood physically; ii) are well understood, but not well calibrated by existing data; or iii) must be simplified to make the calculation method computationally manageable. In some cases these compromises maintain the accuracy of the results for most applications, but reduce accuracy for certain unusual geometric situations or exposure histories. In other cases, we do not know the effect of these compromises on the accuracy of the results. Here we review the important simplifications in our method that may lead to inaccurate results in some situations.

*Height-pressure relationships.* The strong dependence of production rate on atmospheric pressure makes this one of the most important potential inaccuracies for exposure dating. Users who are working in areas where the pressure-height relationship differs significantly from the standard atmosphere should consider using pressure measurements from local meteorological stations, or regional climate model output, rather than a global approximation. Stone (2000), Licciardi et al. (2006), Staiger et al. (2007), and others discuss this in more detail.

*Geometric shielding of sample sites*. The geometric situation at and near a sample site affects nuclide production at the site in two ways. First, shielding due to large-scale topography reduces the cosmic-ray flux that arrives at the sample site. Second, differences between the small-scale geometry of the sample site and the infinite flat surface usually assumed in production rate calculations are predicted to reduce the production rate in the sample due to secondary particle leakage (e.g., Dunne et al., 1999; Masarik and Wieler, 2003; Lal and Chen, 2005). This means that both the surface production rate itself and the production rate - depth profile may differ from the ideal at heavily shielded, steeply dipping, or severely concave or convex sample locations. In keeping with common practice, as discussed above, we greatly simplify this part of the calculation by using only a single shielding factor that takes account of large-scale topographic obstructions only and relies on a standardized angular distribution of cosmic radiation at the surface. Our method may have systematic inaccuracies for samples collected on steeply dipping surfaces (greater than approximately 30°) or in heavily shielded locations (e.g., at the foot of cliffs or in slot canyons). Users who seek to collect samples in these pathological situations should consider this issue further. Dunne et al. (1999), Masarik and Wieler (2003), and Lal and Chen (2005) discuss it in more detail.

*Very thick samples or subsurface samples.* Parts of the exposure age and erosion rate calculations involve linear or exponential approximations for the depth-dependence of nuclide production by muon interactions. These approximations improve the speed of the calculation without sacrificing accuracy for the vast majority of applications in which a relatively thin ($<\sim$20 cm) sample is collected at the surface, but they may be inaccurate if used to calculate ages or erosion rates from samples that either are very thick or were collected well below the surface. The user interface is not designed to support subsurface samples, so users could only encounter this limitation if, for example, they attempted to simulate the effects of sample depth below the surface by applying a large topographic shielding factor (this approach

would also cause errors because of the fact that the topographic shielding factor is only applied to spallogenic production). However, users who seek to adapt the MATLAB source code for depth-profile applications should investigate this issue closely.

*Cross-sections for nuclide production by fast muon interactions*. Cross-sections for fast muon reactions depend strongly on muon energy. The values of these cross-sections that we use (from Heisinger et al., 2002b) were measured at muon energies $> 70$ GV. As the mean energy of muons at ground level is near 10 GV, this requires a large extrapolation in muon energy. It appears that production rates predicted by these cross-section measurements overestimate $^{26}$Al and $^{10}$Be concentrations measured in deep rock cores (Stone et al., 1998b, unpublished measurements by Stone), but the reason for this mismatch is unclear. Thus, our method may systematically overestimate erosion rates when they are extremely high (greater than ca. 0.5 cm $\cdot$ yr$^{-1}$).

*Application to watershed-scale erosion rates*. Many erosion-rate studies seek to infer watershed-scale erosion rates from cosmogenic-nuclide concentrations in river sediment (e.g., von Blanckenburg, 2006; Bierman and Nichols, 2004). The method described and implemented here is designed for calculating surface erosion rates at a particular site and not for calculating basin-scale erosion rates. A strictly correct calculation of the basin-scale erosion rate requires a complete representation of the basin topography, which cannot be submitted to the present calculators. If supplied with the mean latitude and elevation of the watershed, however, the method described here will yield approximately correct results. For watersheds that do not span a large elevation range and otherwise satisfy the assumptions of the method, the error arising from using this approximation instead of a strictly correct areally-averaged production rate will be only a few percent. In reality, this uncertainty is likely to be small relative to the uncertainty contributed by the many other assumptions that are required to calculate a basin-scale erosion rate. However, users who seek very accurate basin-scale erosion rates, or are working in high-relief basins, should consider this in more detail.

## 4 Future improvements

It is certain that the calculation methods that we have used here will be superseded by improved methods in future. The most important improvements, which are the subject of active research at present, are likely to be i) improvements in scaling production rates for elevation, ii) improved models of past magnetic field variations; and iii) more accurate and more geographically widespread calibration measurements. Future versions of this calculator, that take these improvements into account, will yield different results for the same measurements of nuclide concentrations. Once again, this highlights the importance of reporting all the observations

and measurements that are needed to recalculate published results using improved methods.

## 5 Acknowledgements

The contributions of G. Balco, J. Stone, and N. Lifton to this work are part of the CRONUS-Earth project, and were supported by NSF grant EAR-0345574. T. Dunai's contribution to this work was part of the CRONUS-EU project and was supported by EU grant MC-RTN-511927. Dan Farber, Bob Finkel, Brent Goehring, Kuni Nishiizumi, Lewis Owen, Bill Phillips, and Joerg Schaefer provided valuable help in developing and testing the overall approach, the MATLAB code, and the user interface. The manuscript was reviewed by Fred Phillips and an anonymous reviewer. John Gosse was the editor.

## References

Ackert, R., Singer, B., Guillou, H., Kaplan, M., Kurz, M., 2003. Long-term cosmogenic $^{3}$He production rates from $^{40}$Ar/$^{39}$Ar and K-Ar dated Patagonian lava flows at 47°S. Earth and Planetary Science Letters 210, 119–136.

Bevington, P., Robinson, D., 1992. Data Reduction and Error Analysis for the Physical Sciences. WCB McGraw-Hill.

Bierman, P., Nichols, K., 2004. Rock to sediment – slope to sea with $^{10}$Be – rates of landscape change. Annual Reviews of Earth and Planetary Sciences 32, 215–255.

Blard, P.-H., Pik, R., Lavè, J., Bourlès, D., Burnard, P., Yokochi, R., Marty, B., Trusdell, F., 2006. Cosmogenic $^{3}$He production rates revisited from evidences of grain size dependent release of matrix-sited helium. Earth and Planetary Science Letters 247, 222–234.

Boezio, M., Carlson, P., Francke, T., Weber, N., Sufffert, M., Hof, M., Menn, W., Simon, M., Stephens, S., Bellotti, R., Cafagna, F., Circella, M., DeMarzo, C., Finetti, N., Papini, P., Piccardi, S., Spilllantini, P., Ricci, M., Casolino, M., DePascale, M., Morselli, A., Picozza, P., Sparvoli, R., Barbiellini, G., Schiavon, P., Vacchi, A., Zampa, N., Grimani, C., Mitchell, J., Ormes, J., Streitmatter, R., Bravar, U., Golden, R., Stochaj, S., 2000. Measurement of the flux of atmospheric muons with the CAPRICE94 apparatus. Physical Review D 62 (032007).

Cerling, T., Craig, H., 1994. Cosmogenic $^{3}$He production rates from 39°N to 46°N latitude, western USA and France. Geochimica Et Cosmochimica Acta 58, 249–255.

Desilets, D., Zreda, M., 2003. Spatial and temporal distribution of secondary cosmic-ray nucleon intensities and applications to in-situ cosmogenic dating. Earth and Planetary Science Letters 206, 21–42.

Desilets, D., Zreda, M., Prabu, T., 2006. Extended scaling factors for in situ cosmogenic nuclides: New measurements at low latitude. Earth and Planetary Science Letters 246, 265–276.

Dunai, T., 2000. Scaling factors for production rates of in situ produced cosmogenic nuclides: a critical reevaluation. Earth and Planetary Science Letters 176 (157-169).

Dunai, T., 2001. Influence of secular variation of the magnetic field on production rates of in situ produced cosmogenic nuclides. Earth and Planetary Science Letters 193, 197–212.

Dunai, T., Wijbrans, J., 2000. Long-term cosmogenic $^{3}$He production rates (152 ka - 1.35 Ma) from $^{40}$Ar/$^{39}$Ar dated basalt flows at 29°N latitude. Earth and Planetary Science Letters 176, 147–156.

Dunne, J., Elmore, D., Muzikar, P., 1999. Scaling factors for the rates of production of cosmogenic nuclides for geometric shielding and attenuation at depth on sloped surfaces. Geomorphology 27, 3–12.

Farber, D., Hancock, G., Finkel, R., Rodbell, D., 2005. The age and extent of tropical alpine glaciation in the Cordillera Blanca, Peru. Journal of Quaternary Science 20, 759–776.

Gosse, J., Klein, J., 1996. Production rate of *in-situ* cosmogenic $^{10}$Be in quartz at high altitude and mid latitude. Radiocarbon 38, 154–155.

Gosse, J. C., Evenson, E., Klein, J., Lawn, B., Middleton, R., 1995. Precise cosmogenic $^{10}$Be measurements in western North America: support for a global Younger Dryas cooling event. Geology 23, 877–880.

Gosse, J. C., Phillips, F. M., 2001. Terrestrial in situ cosmogenic nuclides: theory and application. Quaternary Science Reviews 20, 1475–1560.

Granger, D., Riebe, C., Kirchner, J., Finkel, R., 2001. Modulation of erosion on steep granitic slopes by boulder armoring, as revealed by cosmogenic $^{26}$Al and $^{10}$Be. Earth and Planetary Science Letters 186, 269–281.

Guyodo, Y., Valet, J.-P., 1999. Global changes in intensity of the Earth's magnetic field during the past 800 kyr. Nature 399, 249–252.

Heisinger, B., Lal, D., Jull, A. J. T., Kubik, P., Ivy-Ochs, S., Knie, K., Nolte, E., 2002a. Production of selected cosmogenic radionuclides by muons: 2. Capture of negative muons. Earth and Planetary Science Letters 200 (3-4), 357–369.

Heisinger, B., Lal, D., Jull, A. J. T., Kubik, P., Ivy-Ochs, S., Neumaier, S., Knie, K., Lazarev, V., Nolte, E., 2002b. Production of selected cosmogenic radionuclides by muons 1. Fast muons. Earth and Planetary Science Letters 200 (3-4), 345–355.

Korte, M., Constable, C., 2005a. Continuous geomagnetic field models for the past 7 millenia: 2. CALS7K. Geochemistry, Geophysics, Geosystems 6, Q02H16.

Korte, M., Constable, C., 2005b. The geomagnetic dipole moment over the last 7000 years – new results from a global model. Earth and Planetary Science Letters 236, 348–358.

Kubik, P., Ivy-Ochs, S., 2004. A re-evaluation of the 0-10 ka $^{10}$Be production rate for exposure dating obtained from the Köfels (Austria) landslide. Nuclear Instruments and Methods in Physics Research B 223-224, 618–622.

Kubik, P., Ivy-Ochs, S., Masarik, J., Frank, M., Schluchter, C., 1998. $^{10}$Be and $^{26}$Al production rates deduced from an instantaneous event within the dendrocalibration curve, the landslide of Köfels, Ötz Valley, Austria. Earth and Planetary Science Letters 161, 231–241.

Kurz, M., Colodner, D., Trull, T., Moore, R., O'Brien, K., 1990. Cosmic ray exposure dating with in situ produced cosmogenic $^{3}$He: results from young Hawaiian lava flows. Earth and Planetary Science Letters 97, 177–189.

Lal, D., 1991. Cosmic ray labeling of erosion surfaces: in situ nuclide production rates and erosion models. Earth Planet. Sci. Lett. 104, 424–439.

Lal, D., Chen, J., 2005. Cosmic ray labeling of erosion surfaces II: Special cases of exposure histories of boulders, soil, and beach terraces. Earth and Planetary Science Letters 236, 797–813.

Larsen, P., 1996. In-situ production rates of cosmogenic $^{10}$Be and $^{26}$Al over the past 21,500 years determined from the terminal moraine of the Laurentide Ice Sheet, north-central New Jersey. Ph.D. thesis, University of Vermont.

Licciardi, J., Kurz, M., Clark, P., Brook, E., 1999. Calibration of cosmogenic $^{3}$He production rates from Holocene lava flows in Oregon, USA, and effects of the Earth's magnetic field. Earth and Planetary Science Letters 172, 261–271.

Licciardi, J., Kurz, M., Curtice, J., 2006. Cosmogenic $^{3}$He production rates from Holocene lava flows in Iceland. Earth and Planetary Science Letters 246, 251–264.

Lifton, N., Bieber, J., Clem, J., Duldig, M., Evenson, P., Humble, J., Pyle, R., 2005. Addressing solar modulation and long-term uncertainties in scaling secondary cosmic rays for in situ cosmogenic nuclide applications. Earth and Planetary Science Letters 239, 140–161.

Lifton, N., Smart, D., Shea, M., 2007 in review. Scaling time-integrated in situ cosmogenic nuclide production rates using a continuous geomagnetic model. Earth and Planetary Science Letters.

Masarik, J., Wieler, R., 2003. Production rates of cosmogenic nuclides in boulders. Earth and Planetary Science Letters 216, 201–208.

Nishiizumi, K., 2002. $^{10}$Be, $^{26}$Al, $^{36}$Cl, and $^{41}$Ca AMS standards: Abstract O16-1. In: 9th Conference on Accelerator Mass Spectrometry. p. 130.

Nishiizumi, K., 2004. Preparation of $^{26}$Al AMS standards. Nuclear Instruments and Methods in Physics Research B 223-224, 388–392.

Nishiizumi, K., Finkel, R., Klein, J., Kohl, C., 1996. Cosmogenic production of $^{7}$Be and $^{10}$Be in water targets. Journal of Geophysical Research 101 (B10), 22,225–22,232.

Nishiizumi, K., Imamura, M., Caffee, M., Southon, J., Finkel, R., McAnich, J., 2007. Absolute calibration of $^{10}$Be AMS standards. Nuclear Instruments and Methods in Physics Research B 258, 403–413.

Nishiizumi, K., Winterer, E., Kohl, C., Klein, J., Middleton, R., Lal, D., Arnold, J., 1989. Cosmic ray production rates of $^{26}$Al and $^{10}$Be in quartz from glacially polished rocks. J. Geophys. Res. 94, 17,907–17,915.

Radok, U., Allison, I., Wendler, G., 1996. Atmospheric surface pressure over the interior of Antartica. Antarctic Science 8, 209–217.

Reimer, P., Baillie, M., Bard, E., Bayliss, A., Beck, J., Bertrand, C., Blackwell, P., Buck, C., Burr, G., Cutler, K., Damon, P., Edwards, R., Fairbanks, R., Friedrich, M., Guilderson, T., Hogg, A., Hughen, K., Kromer, B., McCormac, G., Manning, S., Ramsey, C., Reimer, R., Remmele, S., Southon, J., Stuiver, M., Talamo, S., Taylor, F., van der Plicht, J., Weyhenmeyer, C., 2004. INTCAL04 terrestrial radiocarbon age calibration, 0-26 cal kyr bp. Radiocarbon 46, 1029–1058.

Staiger, J., Gosse, J., Toracinta, R., Oglesby, B., Fastook, J., Johnson, J., 2007. Atmospheric scaling of cosmogenic nuclide production: climate effect. Journal of Geophysical Research 112, BO2205.

Stone, J., Ballantyne, C., Fifield, L., 1998a. Exposure dating and validation of periglacial weathering limits, northwest Scotland. Geology 26, 587–590.

Stone, J. O., 2000. Air pressure and cosmogenic isotope production. Journal of Geophysical Research 105 (B10), 23753–23759.

Stone, J. O. H., Evans, J. M., Fifield, L. K., Allan, G. L., Cresswell, R. G., 1998b. Cosmogenic chlorine-36 production in calcite by muons. Geochimica Et Cosmochimica Acta 62 (3), 433–454.

von Blanckenburg, F., 2006. The control mechanisms of erosion and weathering at basin scale from cosmogenic nuclides in river sediment. Earth and Planetary Science Letters 242, 224–239.

Wallner, A., Ikeda, Y., Kutschera, W., Priller, A., Steier, P., Vonach, H., Wild, E., 2000. Precision and accuracy of $^{26}$Al measurements at VERA. Nuclear Instruments and Methods in Physics Research B 172, 382–387.

Yang, S., Odah, H., Shaw, J., 2000. Variations in the geomagnetic dipole moment over the last 12,000 years. Geophysical Journal International 140, 158–162.

Table 1
Measurements and observations needed to calculate an exposure age or erosion rate.

| Field | Units | Comments |
|---|---|---|
| Sample name | Text | |
| Latitude | Decimal degrees | South latitudes are negative. |
| Longitude | Decimal degrees | West longitudes are negative; longitudes should be between -180°and 180°. |
| Elevation (atmospheric pressure) | m (hPa) | Sample elevation can be specified as either meters above sea level or as mean atmospheric pressure at the site. If elevation is given, one must also select an atmosphere approximation to use for calculating the atmospheric pressure. Two are available: the standard atmosphere equation with geographically variable surface pressure and 1000 mb temperature (see text for details) and one designed for Antarctica (see Stone, 2000, for discussion). |
| Sample thickness | cm | |
| Sample density | $g \cdot cm^{-3}$ | |
| Shielding correction | nondimensional, between 0 and 1 | Ratio of the production rate at the obstructed site to the production rate at a site at the same location and elevation, but with a flat surface and a clear horizon. We provide a separate calculator to obtain the shielding correction from the measured horizon geometry. |
| Erosion rate | $cm \cdot yr^{-1}$ | The erosion rate of the sample surface inferred from independent evidence, to be taken into account when computing the exposure age. Only required for exposure-age calculations. |
| Nuclide concentrations | $atoms \cdot g^{-1}$ | $^{10}$Be and $^{26}$Al concentrations in quartz in the sample. Should be normalized to the $^{10}$Be standard of Nishiizumi (2002) and the $^{26}$Al standard of Nishiizumi (2004) (see text for discussion). Should account for laboratory process and carrier blanks. |
| Uncertainties in nuclide concentrations | $atoms \cdot g^{-1}$ | 1-standard error analytical uncertainties in the measured nuclide concentrations. Should account for all sources of analytical error, including AMS measurement uncertainty, Al or Be concentration measurement uncertainty, and blank uncertainty. |

Table 2
Results of an exposure age calculation.

| Field | Units | Comments |
|---|---|---|
| Exposure age | years | Reports five exposure ages corresponding to the five scaling schemes. |
| Internal uncertainty | years | The internal uncertainty depends only on measurement error in the nuclide concentration, so it is the same for all scaling schemes. |
| External uncertainty | years | Reports five values corresponding to the five scaling schemes. |
| Thickness scaling factor | nondimensional | Ratio of the production rate in the thick sample to the surface production rate. |
| Shielding factor | nondimensional | This value is submitted by the user (see Table 1) – we re-report it in the results for completeness. |
| Surface production rate due to muons | atoms $\cdot$ g$^{-1}\cdot$ yr$^{-1}$ | The production rate from muons is common to all the scaling schemes. |
| Surface production rate due to spallation for the St scaling scheme | atoms $\cdot$ g$^{-1}\cdot$ yr$^{-1}$ | The production rate changes with time in the other four scaling schemes, so we do not report it. Production rate variations for the time-dependent scaling schemes are shown in a separate plot on the single-sample results page. |

Table 3
Results of an erosion rate calculation.

| Field | Units | Comments |
|---|---|---|
| Erosion rate | $g \cdot cm^{-2} \cdot yr^{-1}$ and $m \cdot Myr^{-1}$ | Reports five erosion rates corresponding to the five scaling schemes. |
| Internal uncertainty | $m \cdot Myr^{-1}$ | The internal uncertainty depends only on measurement error in the nuclide concentration, so it is the same for all scaling schemes. |
| External uncertainty | $m \cdot Myr^{-1}$ | Reports five values corresponding to the five scaling schemes. |
| Shielding factor | nondimensional | This value is submitted by the user – we re-report it in the results for completeness. |
| Surface production rate due to muons | $atoms \cdot g^{-1} \cdot yr^{-1}$ | The production rate from muons is common to all the scaling schemes. |
| Surface production rate due to spallation for the St scaling scheme | $atoms \cdot g^{-1} \cdot yr^{-1}$ | The production rate changes with time in the other four scaling schemes, so we do not report it. |

Table 4
List of scaling schemes for spallogenic production. The column marked 'ID' gives the two-letter code that identifies each scaling scheme in tables, figures, the supplementary material, the online documentation, and much of the MATLAB code.

| ID | References | Description |
|---|---|---|
| St | Lal (1991), Stone (2000) | Based on the latitude-altitude scaling factors of Lal (1991), as recast as functions of latitude and atmospheric pressure by Stone (2000). The scaling factor is a function of geographic latitude and atmospheric pressure. Does not take account of magnetic field variations – the nuclide production rate is constant over time. |
| De | Desilets et al. (2006) | The scaling factor is a function of cutoff rigidity and atmospheric pressure. Production rates vary with time according to magnetic field changes. |
| Du | Dunai (2001) | The scaling factor is a function of cutoff rigidity and atmospheric pressure. Production rates vary with time according to magnetic field changes. |
| Li | Lifton et al. (2005) | The scaling factor is a function of cutoff rigidity, atmospheric pressure, and a solar modulation parameter. Production rates vary with time according to changes in solar output as well as changes in the Earth's magnetic field. |
| Lm | Lal (1991), Stone (2000), Nishiizumi et al. (1989) | An adaptation of the Lal (1991) scaling scheme that accomodates paleomagnetic corrections. Production rates vary with time according to magnetic field changes. Based on the paleomagnetic correction described in Nishiizumi et al. (1989). |

Table 5. Magnetic field models used for the paleomagnetically-corrected scaling schemes; method of calculating the cutoff rigidity from the magnetic field model. For a given time period, the magnetic field model itself is the same for all of the scaling schemes. However, the method of calculating the cutoff rigidity and hence the scaling factor from the field model differs between scaling schemes.

| ID | Time period ($10^3$ yr BP) | Field model | Derivative of field model | Method of calculating cutoff rigidity $R_C$ |
|---|---|---|---|---|
| De | 0-7 | Spherical harmonic field model of Korte and Constable (2005a) | $R_C$ from trajectory tracing (Lifton et al., 2007 in review) | Directly assigned |
| | 7-12 | GAD[1] with dipole moment from Yang et al. (2000) | $M/M_0$, the ratio of past to present dipole moment, by normalizing to 1950 Definitive Geomagnetic Reference Field (DGRF) | Equation (19) of Desilets and Zreda (2003), using geographic latitude as input |
| | 12- 800 | GAD with dipole moment from SINT800 record (Guyodo and Valet, 1999) | ” | ” |
| | $>$ 800 | GAD with mean intensity of SINT800 record | ” | ” |
| Du | 0-7 | Spherical harmonic field model of Korte and Constable (2005a) | Magnetic inclination and horizontal field strength | Equation (2) of Dunai (2001). |
| | 7-12 | GAD with dipole moment from Yang et al. (2000) | $M/M_0$, the ratio of past to present dipole moment, by normalizing to 1950 DGRF | Equation (1) of Dunai (2001) |
| | 12- 800 | GAD with dipole moment from SINT800 record (Guyodo and Valet, 1999) | ” | ” |
| | $>$ 800 | GAD with mean intensity of SINT800 record | ” | ” |
| Li | 0-7 | Spherical harmonic field model of Korte and Constable (2005a) | $R_C$ from trajectory tracing (Lifton et al., 2007 in review) | Directly assigned |
| | 7-12 | GAD with dipole moment from Yang et al. (2000) | $M/M_0$, the ratio of past to present dipole moment, by normalizing to 1950 DGRF | Equation (6) of Lifton et al. (2005), using geographic latitude as input |
| | 12- 800 | GAD with dipole moment from SINT800 record (Guyodo and Valet, 1999) | ” | ” |
| | $>$ 800 | GAD with mean intensity of SINT800 record | ” | ” |
| Lm | 0-7 | Spherical harmonic field model of Korte and Constable (2005a) | Pole position and dipole moment derived from approximating the complete field by a geocentric dipole (Korte and Constable, 2005b) | Equation (1) of Dunai (2001), using geomagnetic latitude as input |
| | 7-12 | GAD with dipole moment from Yang et al. (2000) | $M/M_0$, the ratio of past to present dipole moment, by normalizing to 1950 DGRF | Equation (1) of Dunai (2001), using geographic latitude as input. |
| | 12- 800 | GAD with dipole moment from SINT800 record (Guyodo and Valet, 1999) | ” | ” |
| | $>$ 800 | GAD with mean intensity of SINT800 record | ” | ” |

[1] GAD: geocentric axial dipole.

Table 6. Reference production rates for spallation $P_{ref,sp}$ (atoms $\cdot$ g$^{-1}\cdot$ yr$^{-1}$) inferred from the calibration data set for the five scaling schemes, and reduced chi-square statistics describing the fit of each scaling scheme and corresponding reference production rate to the individual calibration measurements. The averaging procedure for computing the reference production rates weights all calibration sites, rather than all samples, equally in order to reduce over-weighting of sites where more samples were measured. The reduced chi-squared values, on the other hand, reflect the goodness of fit to the entire data set , not the site averages alone.

| ID | $^{10}$Be | | $^{26}$Al$^{(1)}$ | | $^{26}$Al$^{(2)}$ | | $^{3}$He | |
|---|---|---|---|---|---|---|---|---|
| | $P_{ref,sp}$ | $\chi^2_R$ | $P_{ref,sp}$ | $\chi^2_R$ | $P_{ref,sp}$ | $\chi^2_R$ $^{(3)}$ | $P_{ref,sp}$ | $\chi^2_R$ |
| St | 4.96 $\pm$ 0.43 (9%) | 2.8 | 30.6 $\pm$ 1.6 (5%) | 2.9 | 30.2 $\pm$ 2.6 (9%) | 2.8 | 107 $\pm$ 16 (15%) | 9.1 |
| De | 4.88 $\pm$ 0.56 (11%) | 13 | 29.8 $\pm$ 1.3 (4%) | 2.9 | 29.8 $\pm$ 3.4 (11%) | 2.9 | 114 $\pm$ 14 (12%) | 6.7 |
| Du | 4.90 $\pm$ 0.56 (11%) | 10 | 29.8 $\pm$ 1.3 (4%) | 2.9 | 29.9 $\pm$ 3.4 (11%) | 2.9 | 113 $\pm$ 15 (13%) | 7.2 |
| Li | 5.39 $\pm$ 0.52 (10%) | 10 | 32.1 $\pm$ 1.8 (6%) | 3.1 | 32.9 $\pm$ 3.2 (10%) | 3.1 | 122 $\pm$ 14 (11%) | 6.1 |
| Lm | 4.84 $\pm$ 0.41 (8%) | 3.6 | 29.7 $\pm$ 1.3 (4%) | 2.8 | 29.6 $\pm$ 2.5 (8%) | 2.8 | 106 $\pm$ 14 (13%) | 8.4 |

(1) Calculated from $^{26}$Al calibration data set.
(2) Calculated from $^{10}$Be calibration data set with $^{26}$Al/$^{10}$Be = 6.1. This value is used in the $^{26}$Al calculators.
(3) With respect to the $^{26}$Al data set.

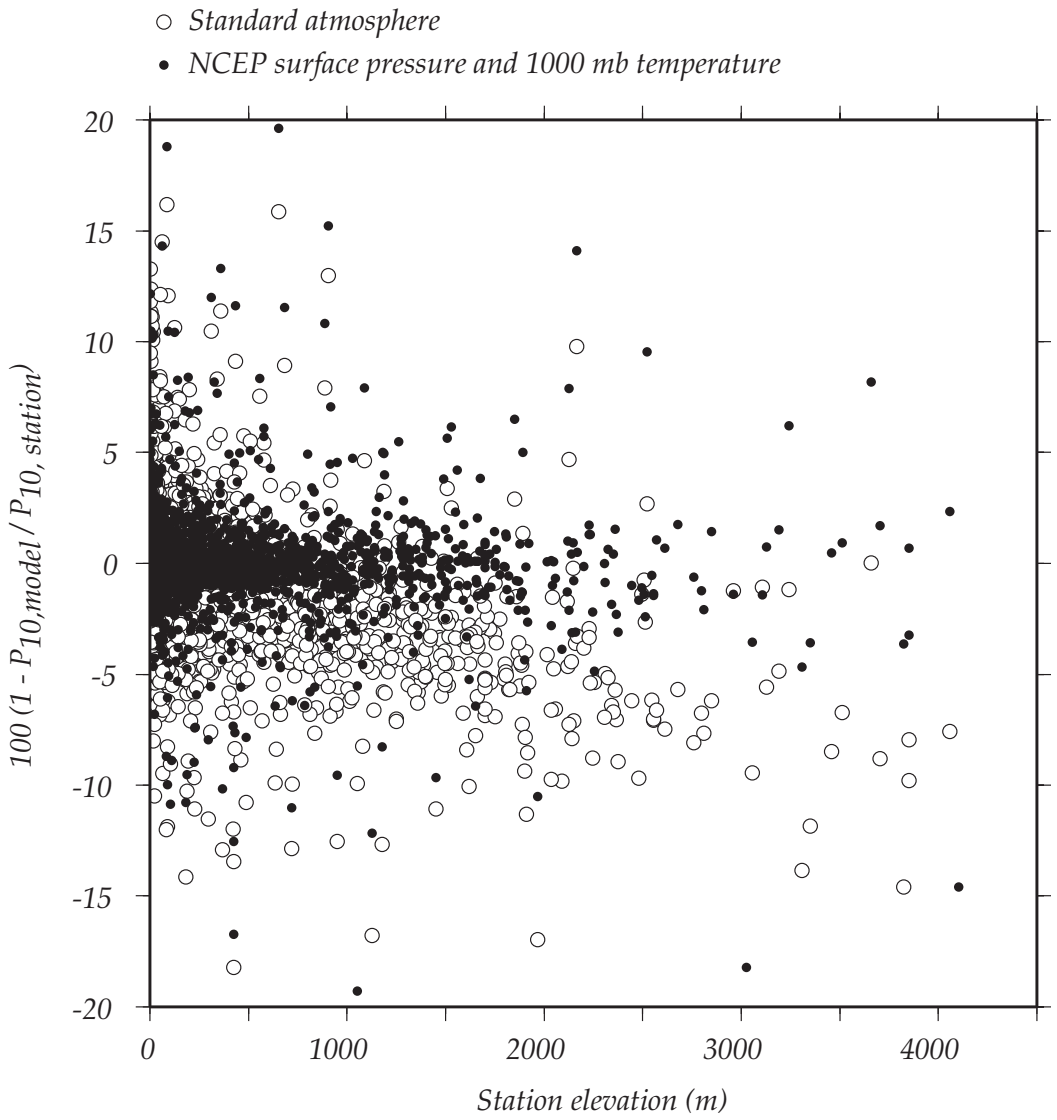


Fig. 1. Effect of atmospheric pressure - elevation approximations on production rate estimates. The data on this figure show $^{10}$Be production rates estimated for the locations of meteorological stations in the NCAR World Monthly Surface Station Climatology data set (see text for details). Stations south of 60°S are not included.The y-axis shows the percentage difference between the $^{10}$Be production rates $P_{10,model}$ and $P_{10,station}$, where $P_{10,model}$ is the production rate given the mean atmospheric pressure estimated from the location and elevation of the station and a global pressure-elevation relationship, and $P_{10,station}$ is the production rate given the mean atmospheric pressure actually recorded at the station. The St scaling scheme is used here; other scaling schemes yield equivalent results. For the open circles, $P_{10,model}$ was calculated using the ICAO standard atmosphere, which systematically underestimates production rates at high elevations. For the closed circles, $P_{10,model}$ was estimated using our default atmospheric pressure-elevation relationship (that draws sea level pressure and 1000 mb temperature from the NCEP reanalysis, as described in the text). Our default elevation-pressure relationship reduces scatter and corrects the systematic bias. We removed obvious errors from the climatology data (for example, where one or more months were missing from the annual average, or where the station elevation was grossly in error), but did not make a comprehensive effort to screen the data set further. Thus, some of the outliers in this figure probably reflect errors in the reported station pressures.

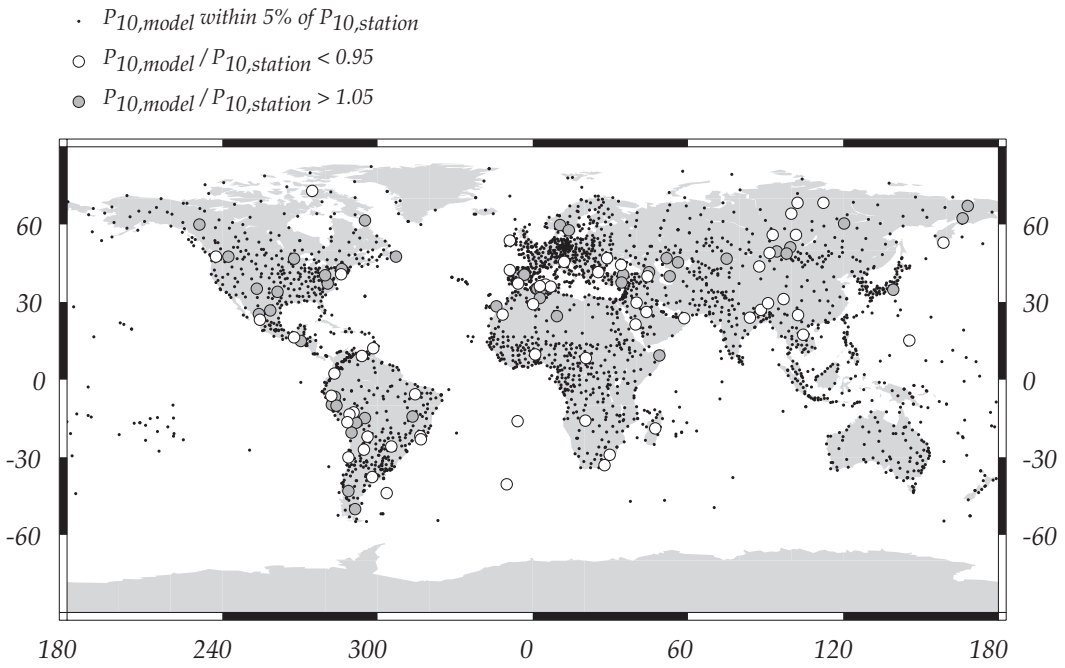


Fig. 2. Geographic representation of the accuracy of the atmospheric pressure - elevation relationship used in the online calculator. The points on the map are the locations of meteorological stations in the NCAR World Monthly Surface Station Climatology data set (see text for details). The same data are shown in Figure 1. The small dots show stations where the $^{10}$Be production rate estimated from the location of the station and our default atmospheric pressure-elevation relationship (that draws sea level pressure and 1000 mb temperature from the NCEP reanalysis, as described in the text) is within 5% of the $^{10}$Be production rate estimated from the mean atmospheric pressure actually recorded at the station. White circles show stations where the production rate calculated using our pressure-elevation relationship is more than 5% lower than the production rate calculated from the actual station pressure; gray circles show stations where is is more than 5% higher. Stations south of 60°S are not included. As discussed in the caption for Figure 1, we did not make a comprehensive effort to screen the data set for errors. Thus, this figure is intended only as a general guideline to identify regions where the default pressure-elevation relationship in the calculators may result in inaccurate exposure ages.

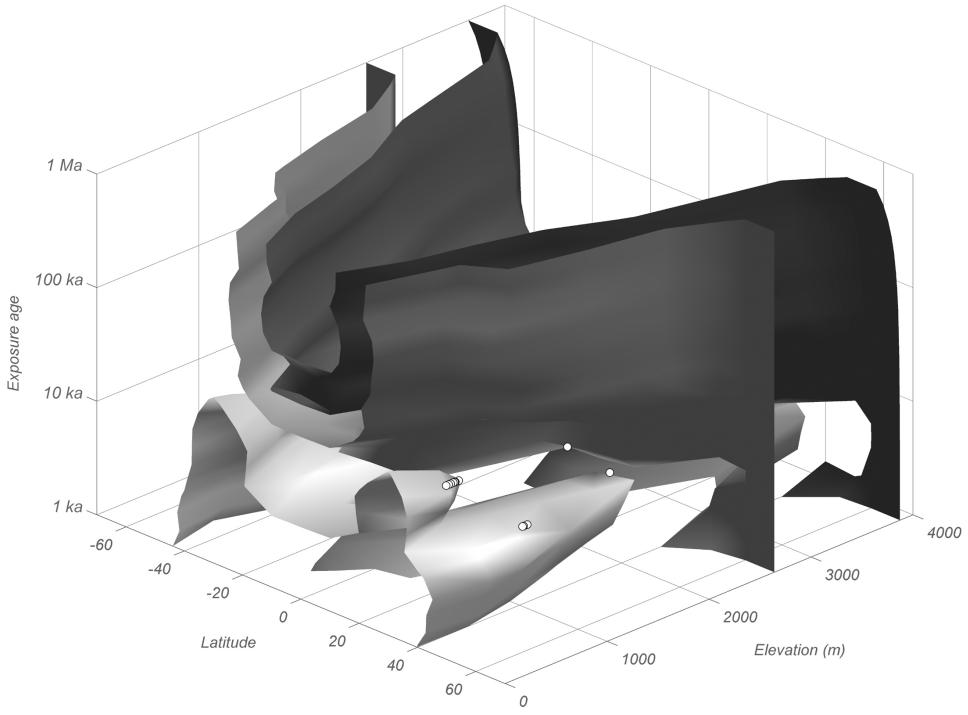


Fig. 3. Difference in exposure ages generated by the St and De scaling schemes. Here we have calculated exposure ages according to the St and De scaling schemes for a range of latitudes, elevations, and ages. The plot shows three-dimensional contours of the ratio $t_{St}/t_{De}$, where $t_{St}$ is the exposure age according to the St scheme and $t_{De}$ is the exposure age according to the De scheme. The intermediate surface is the $t_{St}/t_{De} = 1$ contour, that is, the set of locations and ages where the two schemes yield the same exposure age. The darker surface is the $t_{St}/t_{De} = 1.1$ contour, that is, the set of locations and ages where the St scaling scheme yields exposure ages 10% higher than the De scaling scheme. The lighter surface is the $t_{St}/t_{De} = 0.9$ contour, that is, the set of locations and ages where the St scaling scheme yields exposure ages 10% lower than the De scaling scheme. The white circles show the locations and ages of samples in the calibration data set. This figure is drawn for 100°W longitude; other meridians would share the same overall characteristics but differ in detail. The important features of this comparison are that $t_{St}/t_{De}$ increases with increasing age because of the paleomagnetic effect, and with increasing elevation because of the different elevation dependences of the production rate.

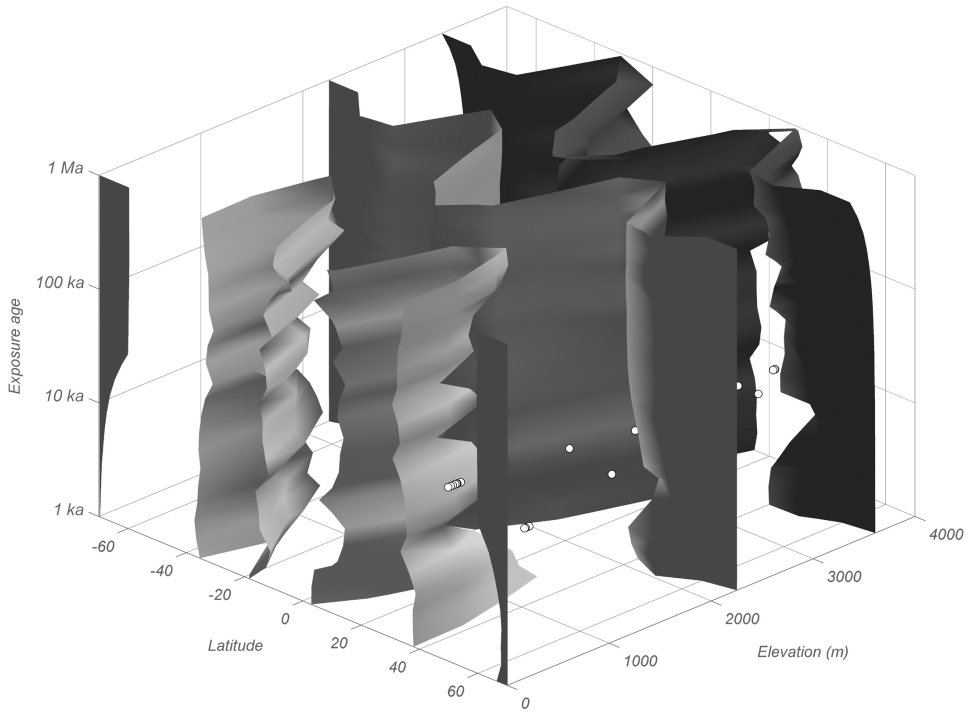


Fig. 4. Difference in exposure ages generated by the Lm and De scaling schemes. The axes, colors, symbols, and assumptions are the same as in Figure 3: the intermediate surface shows $t_{Lm}/t_{De} = 1$,the dark surface shows $t_{Lm}/t_{De} = 1.1$, and the light surface shows $t_{Lm}/t_{De} = 0.9$ Both the Lm and De schemes account for paleomagnetic variations, so the difference between exposure ages calculated with these two schemes does not depend strongly on age. However, Lm and De have different elevation dependences, so $t_{Lm}/t_{De}$ increases with elevation.

Fig. 5. Fit of the five scaling schemes to the $^{10}$Be calibration data set. The left-hand panels show reference production rates for spallation derived by scaling the local, time-integrated production rate obtained from each individual calibration samples to sea level, high latitude, and the present time, plotted against sample elevation. The right-hand panel shows the error-weighted mean and standard error computed from all the estimates of the reference production rate at each calibration site, plotted against the average elevation of all the samples at that site. The horizontal line and gray band show the mean and standard deviation of the summary values for all sites. These are the values we use to calculate exposure ages and erosion rates from $^{10}$Be measurements.

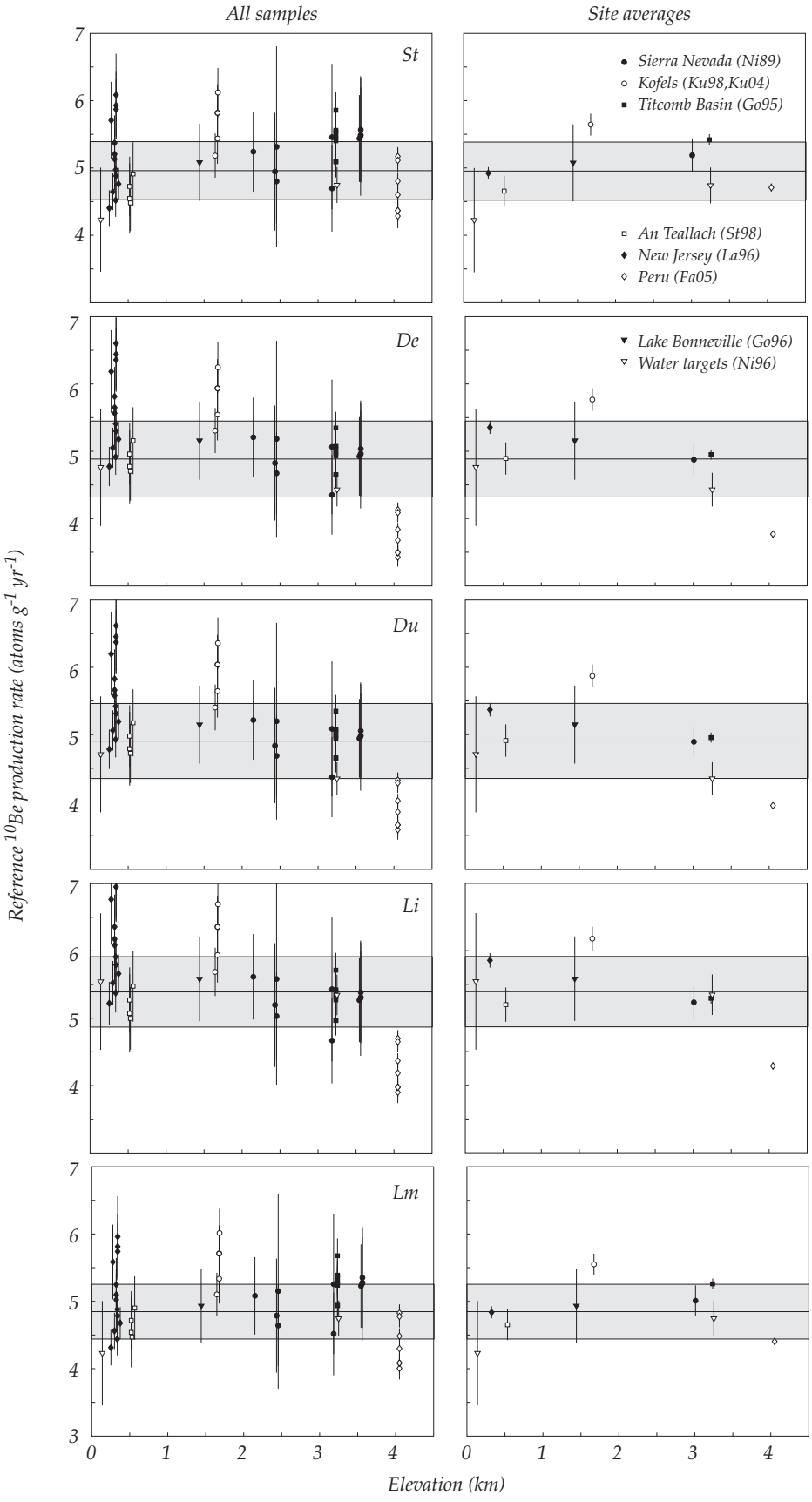
All samples
Site averages
St
De
Du
Li
Lm
Sierra Nevada (Ni89)
Kofels (Ku98,Ku04)
Titcomb Basin (Go95)
An Teallach (St98)
New Jersey (La96)
Peru (Fa05)
Lake Bonneville (Go96)
Water targets (Ni96)
Reference $^{10}$Be production rate (atoms g$^{-1}$ yr$^{-1}$)
Elevation (km)

Fig. 6. Fit of the five scaling schemes to the $^{26}$Al calibration data set. The details of this figure are the same as for Figure 5. As in Figure 5, the horizontal line and gray band show the mean and standard deviation of the summary values for all sites. However, these are not the values actually used to calculate exposure ages and erosion rates from $^{26}$Al measurements. See the text for details.

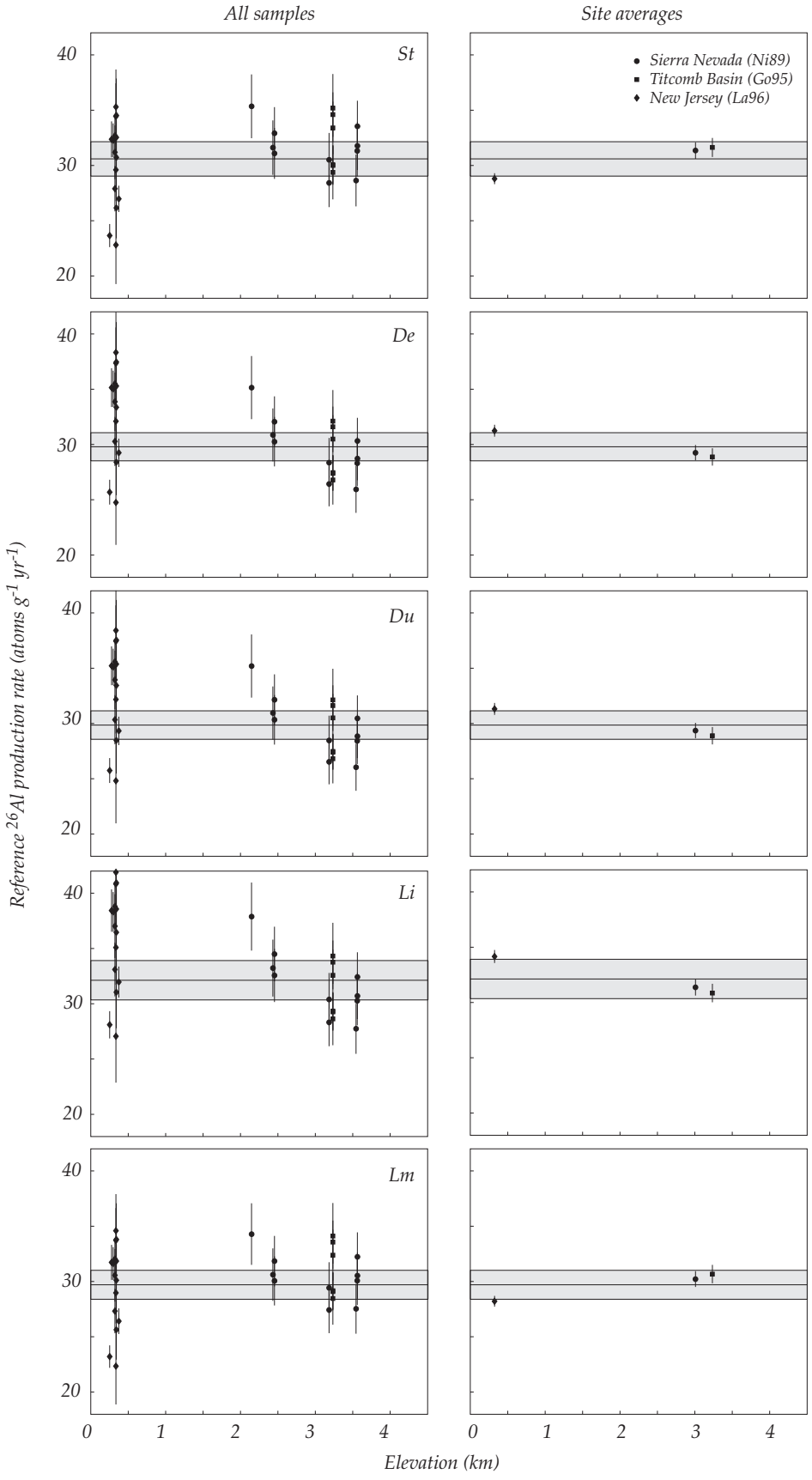
All samples
Site averages
St
De
Du
Li
Lm
Sierra Nevada (Ni89)
Titcomb Basin (Go95)
New Jersey (La96)
40
30
20
0
1
2
3
4
Reference 26Al production rate (atoms g-1 yr-1)
Elevation (km)

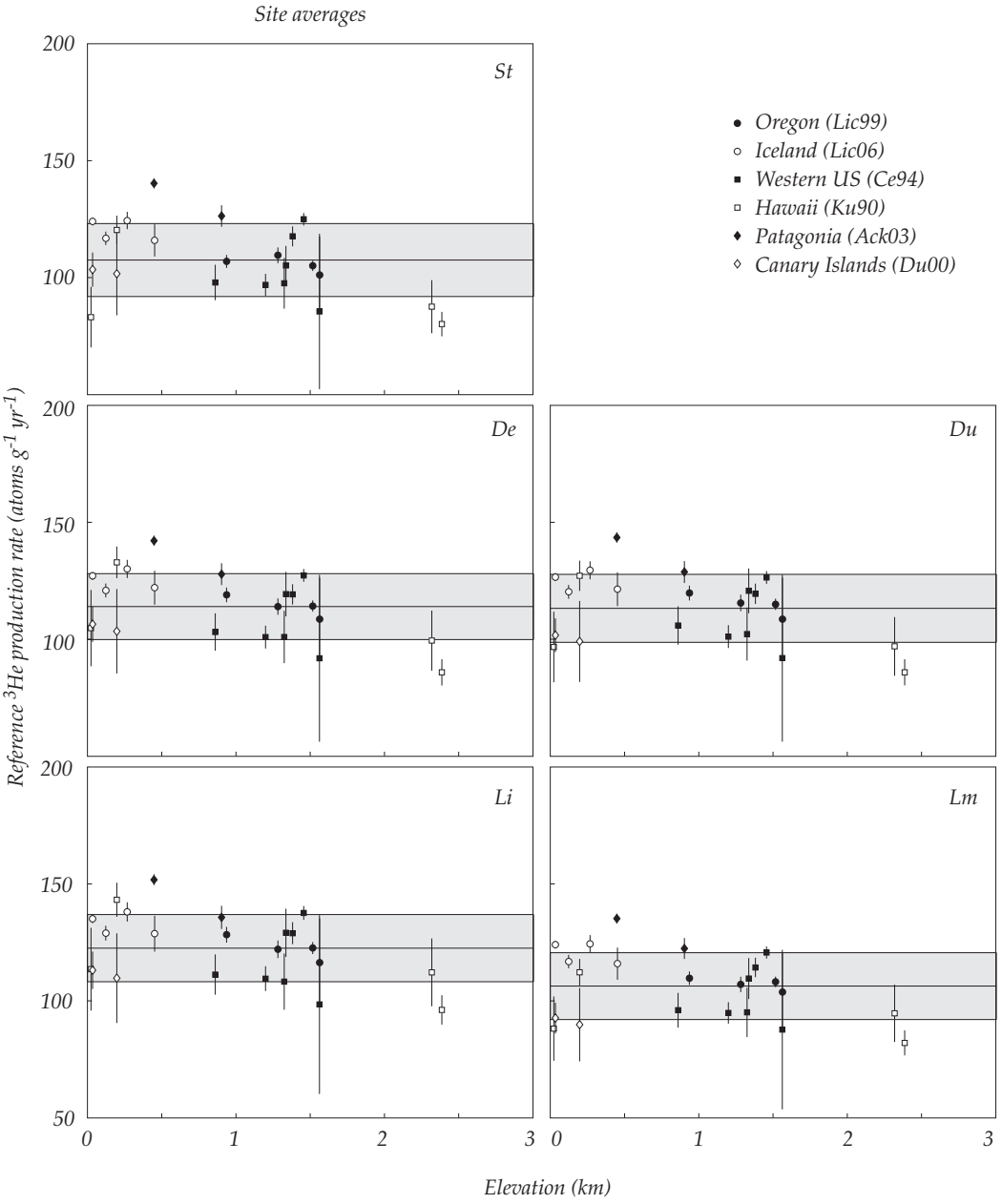


Fig. 7. Fit of the five scaling schemes to the $^3$He calibration data set. Only an error-weighted mean and standard error for each site, and not the full set of measurements from each site, are shown. Note that each of the source papers includes data from multiple sites.

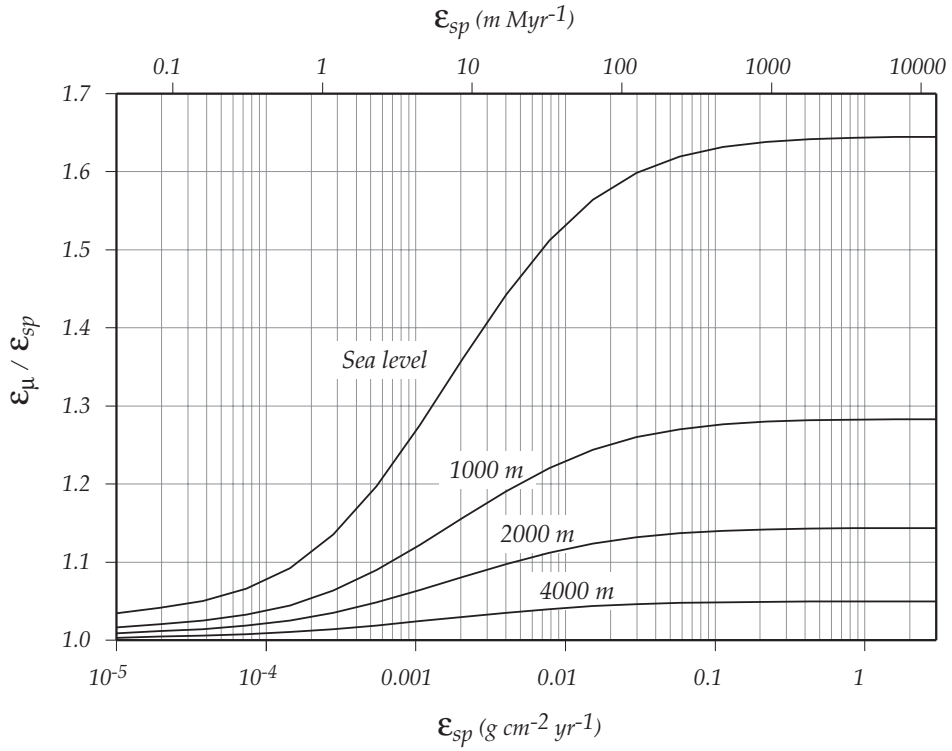


Fig. 8. Difference between calculated erosion rates from a high-latitude sample that take account of subsurface nuclide production by muons ($\epsilon_\mu$; Equation 2) and those that do not ($\epsilon_{sp}$; Equation 3). The two different x-axis scales are related by a density of 2.65 g $\cdot$ cm$^{-3}$.